X-ray imaging of microobjects using dark field refraction-contrast method with resonantly absorbing multilayer mirrors

Vladimir V. Protopopov[*a], Jaroslav Sobota[b], Anton S. Tremsin[c], Oswald H.W. Siegmund[c], Yuriy Ya. Platonov[d]

[a]The Institute of Physics and Technology, Moscow, Russia; [b]Institute of Scientific Instruments, Academy of Sciences of Czech Republic; [c]Space Sciences Laboratory, UC Berkeley, Berkeley, USA; [d]OSMIC Inc., Troy MI, USA;

ABSTRACT

An x-ray multilayer mirror, specially designed to produce resonant absorption at a definite angle of incidence, may be used as an angular dispersive element for refractive x-ray radiography. In this method the signal-to-noise ratio can be significantly enhanced due to suppression of the shot noise produced by the direct beam. Refraction contrast of a copper wire 75 μm in diameter and a human hair was observed using Ni/C multilayer mirror with resonant absorption at CuK_α radiation (1.54Å). The multilayer structure consisting of 30 bilayers was designed for CuK_α radiation so as to have absorbing resonance of the width of about several arc seconds at a grazing angle of 0.8°. A monochromatic probe x-ray beam with a divergence of approximately 5 arc seconds was obtained from a conventional x-ray tube and a double crystal monochromator set in a strongly dispersive configuration. We have developed theoretical basis for this method, and have experimentally proven that it is possible to create critical components for its practical implementation: a multilayer mirror with resonant absorption, an x-ray imaging photon-counting detector with spatial resolution of about several micrometers, and a probe beam with the divergence of several arc seconds. This result proves the feasibility of x-ray refraction radiography using resonantly absorbing multilayer mirrors manufactured by conventional magnetron sputtering technology.

Keywords: X-ray imaging, radiography, refraction, multilayers, detector.

1. INTRODUCTION

X-ray radiography is a widely used technique for obtaining images of inner features of a human body and biological samples. The contrast and spatial resolution of x-ray radiography became extremely important in the past decade due to the problem of cancer diagnostics. Radiation dose is also a very important parameter, determining safety of the technique. Absorption contrast as the basic principle of imaging in traditional x-ray radiography remained essentially unchanged since Roentgen's first experiments a hundred years ago. Therefore, the only way to increase a contrast of small objects in traditional x-ray images is to increase the dose of radiation absorbed by a whole sample. It is well known, however, that this way is unacceptable in medical applications for safety reasons. Today, it is both experimentally and theoretically proven, mainly due to the Ingal group [1,2], that the refractive contrast, originating from the variation of the refractive indices of different parts of a sample, produces far more detailed images of biological tissues, and a variety of imaging techniques for biological and medical investigations based on refraction contrast are being developed using both the coherent synchrotron radiation sources and laboratory x-ray sources. In all of these techniques, sometimes referred to as phase-contrast imaging, the commonly weak useful signal is detected against the background of a strong direct beam. Therefore, the detector shot noise produced by the direct beam decreases the signal-to-noise ratio, which is of a primary importance when an image is recorded electronically. Recently, a new scheme of x-ray refractive radiography was proposed, that can significantly suppress the intensity of a direct beam [3,4] and enhance the signal-to-noise ratio. In this scheme a specially designed multilayer mirror with resonant absorption plays the role of the angular analyzer. In the present paper we discuss the critical components needed for practical implementation of this method.

[*] v.protopopov@mtu-net.ru; Institute of Physics and Technology; Nakhimovskii Pr.34; 117218 Moscow, Russia

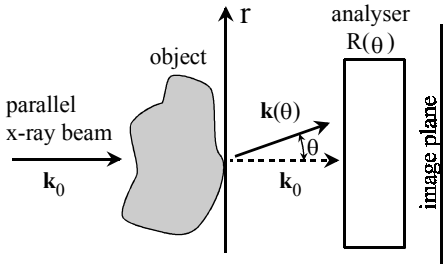

Fig.1. The scheme of the x-ray refractive radiography.

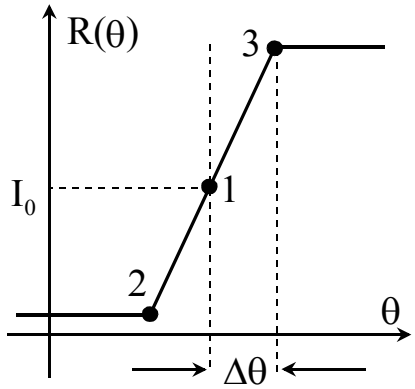

Fig.2 The generalized angular characteristic of a crystal analyzer.

The idea of the x-ray refractive radiography is schematically shown in Fig.1. A parallel x-ray beam with a wave vector $\mathbf{k}_0$ penetrates the object, transparent to x rays. Because of the refraction of x rays on the inner structure of the object, the output beam is composed of the original wave with the vector $\mathbf{k}_0$ and the refracted waves with vectors $\mathbf{k}(\Delta\theta)$ slightly declined from the initial vector $\mathbf{k}_0$. The key part of the scheme is the analyzer, which differentiates the output waves by their direction $\Delta\theta$. In all the schemes used before the role of the analyzer is played by a highly perfect crystal with transmission characteristics in the form of a step function (Fig.2), working in a very narrow angular interval of about a few arc seconds. In order to be sensitive to both directions of the refraction, the working point is usually chosen in the position marked as number 1 in Fig.2. Of course, it is possible to choose any other position as the working point, for instance, 2 or 3, but that will lead to a loss of useful beam energy. Thus, the resultant image registered directly behind the analyzer is formed by the intensity variations $R(\theta)$ proportional to the angle of refraction $\Delta\theta$. Therefore, the resultant intensity distribution in the image plane may be presented in the form of a sum

$$I(\mathbf{r}) = R[\theta(\mathbf{r})] + I_0 \ , \qquad (1)$$

where I_0 is the intensity of the direct beam, which may be much greater than the useful term $R[\theta(\mathbf{r})]$. The direct beam carries practically no information about the object, if the latter is transparent to x rays, and at the same time it deteriorates the image, bringing additional noise into it. For these reasons, the direct beam is undesirable.

It should be mentioned that in recent years, a method of phase-contrast radiography was developed, which requires no analyzer at all[5]. This method is based on the interference of the refracted and direct beams, and, therefore, it demands a very coherent source of extremely high brilliance available today only with the third generation synchrotrons. Therefore, another methods suitable for laboratory applications are welcomed.

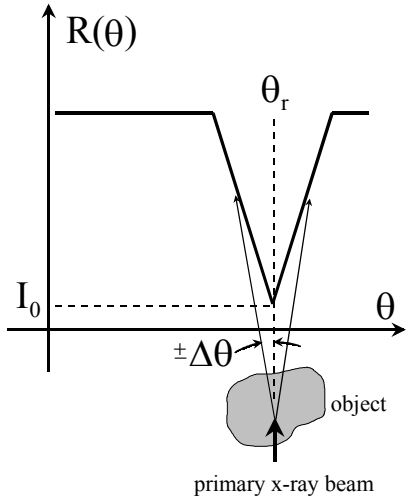

Fig.3. The generalized scheme of a multilayer mirror analyzer.

Suppose now, that the crystal analyzer with the angular characteristic shown in Fig.2 is replaced by a multilayer mirror with the reflection curve shown in Fig.3 in a generalized form. Evidently, the intensity of a direct beam I_0 in this case may be much less, than in the previous case, while the sensitivity of the scheme with respect to the refracted beams is determined by the sharpness of the reflection curve around the resonant angle θ_r. Note that unlike a crystal analyzer, the multilayer analyzer produces symmetrical output for the refracted beams with both positive and negative values of $\Delta\theta$.

2. PHYSICS OF MULTILAYER MIRRORS WITH RESONANT ABSORPTION

Physics of a multilayer mirror with resonant absorption is the same as that of the Fabri-Perrot interferometer. It can be represented as two periodical multilayer mirrors separated by quarter-wave spacer made of weakly absorbing material (Fig.4). Let N be the number of periods in each of the

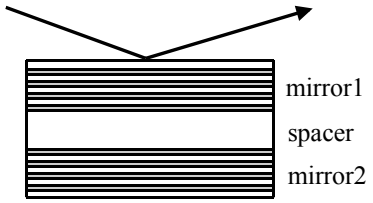

Fig.4. The structure of multilayer mirror with resonant absorption.

two multilayer mirrors, d and d_s the period of multilayer structures and the thickness of the spacer respectively, and $\theta_r = \lambda/2d$ - the grazing angle of the 1st Bragg resonance at the wavelength λ for the two multilayer mirrors. Then the resonant absorption at the angle θ_r takes place when

$$d_s = \frac{2\pi m + \pi}{2k\theta_r} - Nd \ , \tag{1}$$

where $k = 2\pi/\lambda$ is the wave number. In the vicinity of the resonant angle the reflectivity is approximately a quadratic function:

$$R(\theta) = R_0\left[kdN(\theta - \theta_r)\right]^2 = R_0\left[\pi N\frac{\theta - \theta_r}{\theta_r}\right]^2 \ , \tag{2}$$

where R_0 is the maximum reflectivity of the multilayer mirrors at the 1st Bragg resonance. Typical reflection curve for this type of the mirror is presented in Fig.5.

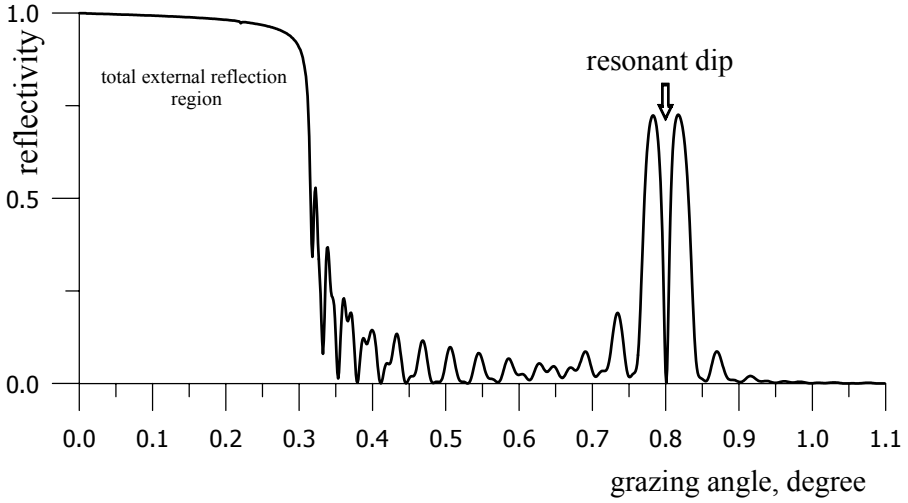

Fig.5. Theoretical reflection curve for Ni/C multilayer mirror with resonant absorption at 0.8°. N =30; λ =1.54Å.

It is clear that in a narrow angular region around the resonant angle the mirror with the reflection curve shown in Fig.5 can play a role of an angular analyzer, as it is shown in Fig.3.

3. NUMERICAL SIMULATION OF THE DARK-FIELD IMAGING

The possible advantage of the dark-field refraction contrast imaging with respect to the traditional absorption radiography can be estimated by means of 3D numerical simulation according to the simplified model shown in fig.6. The case when the image is recorded in the plane P_1 corresponds to traditional absorption radiography, and the case with the image registration in the plane P_2 – to the dark-field refraction contrast imaging. Consider as an object a small ball 50 μm in diameter immersed in water. Angular dispersion of the mirror is determined by the reflection curve shown in Fig.5. The particular numerical values of the resonant dip correspond to the real Ni/C mirror that will be discussed below in the section 5. The results are presented in Fig.7. Left column corresponds to absorption radiography, right – to the dark-field refraction contrast imaging. For heavy materials with strong absorption, such as tungsten, both of these methods give good contrast. But the materials with low absorption, such as carbon, or beta-keratin

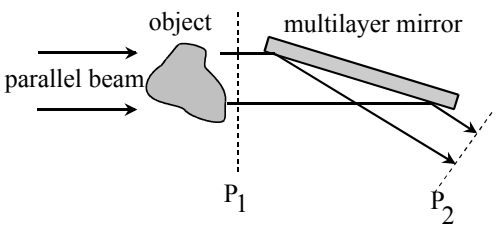

Fig.6. Physical model for numerical simulation.

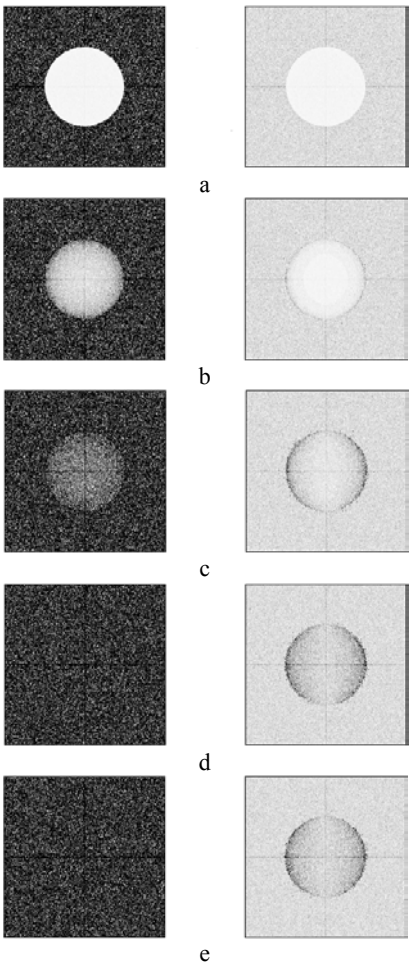

Fig.7. Computer generated images for different materials of the immersed ball: (a) W; (b)Ca; (c) SiO_2; (d) C; (e) β-keratin. Exposure: 200,000 photons. The wavelength 1.54Å.

(protein, the basic component of a human hair), are practically transparent at the wavelength of 1.54Å. Therefore, small objects made of these materials, such as, for example, a ball of 50 μm in diameter, produce practically no absorption contrast. Nevertheless, they can be detected, and their shape can be easily recognized by the dark-field refraction contrast method, as is clear from the right column in Fig.7.

Due to the physics of refraction the maximum deflection of the probe beam, and, consequently, the maximum signal after the angular analyzer will always be in the narrow region near the contour of the object projection onto the image plane. Therefore, refraction contrast imaging stresses the contours of objects. Thus, the spatial resolution of the image detector is of a primary importance. This problem is addressed in the next section.

4. REFRACTION CONTRAST AND SPATIAL RESOLUTION OF THE DETECTOR

Suppose the absorption of the object is negligible, and let the spatial resolution of the detector be equal to Δx . Then maximum detector output signal during imaging of an object in the form of a thread with cross-sectional radius r made of the material with the refraction index n is equal to

$$s \approx I_0 R_0 (kdN)^2 \frac{n}{4} \cdot \left(\frac{2nr}{\Delta x}\right) \ln\left(1 + \frac{\Delta x}{2nr}\right); \quad \Delta x << r \,. \tag{3}$$

Here I_0 is the intensity of the probe beam. It should be noted that in x-ray domain the value of n is very small, typically of the order of 10^{-5} at the wavelength 1.54Å. Therefore, the argument of the logarithm is large compared to unity in all practical cases. Two main conclusions can be drawn from this formula. The first thing is that low spatial resolution, i.e., large Δx , leads to low detector signal. And the second is that the larger the diameter of an object the larger is the signal. In order to estimate quantitatively the practically tolerable value of spatial resolution we shall address the results of numerical simulation presented in Fig.8 for the case of the human hair of 50 μm in diameter. From these data it can be concluded that the spatial resolution must be better than 10 μm for this type of objects.

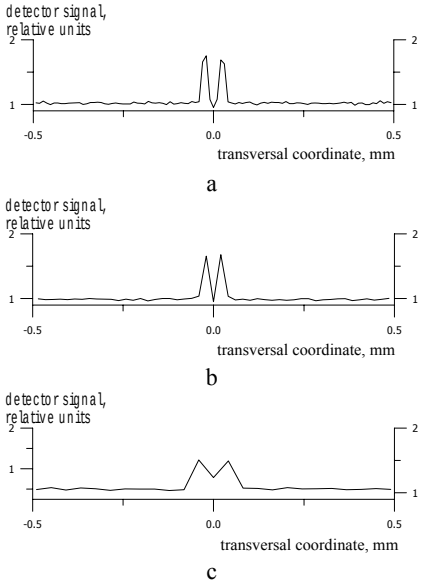

Fig.8. Simulated detector signals for the human hair of 50 μm in diameter: (a) Δx=10 μm; (b) Δx=20 μm; (c) Δx=40 μm. λ =1.54Å.

5. CRITICAL COMPONENTS FOR PRACTICAL IMPLEMENTATION OF THE METHOD

5.1. Multilayer mirror with resonant absorption

We have successfully overcome all technological problems and created Ni/C multilayer mirror with resonant absorption using magnetron sputtering installation LEYBOLD Z550. The mirror structure was designed with the help of the optimization routine from the software package PSoft for the wavelength 1.54Å so as to have the resonance at the grazing angle 0.8°. Multilayer coating consisting of 30 bilayers was deposited on flat quartz substrate 40×40 mm^2

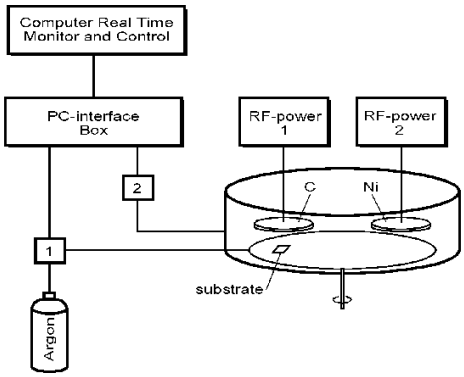

Fig.9. Scheme of the deposition technique: 1- flow controller; 2 -pressure gauge.

with average roughness 6Å and surface shape variation not more than 3 arc seconds. Carefully balanced magnetron sputtering equipment produces random variations of the average layers thickness as small as 0.1÷0.5Å [6].

Sputtering unit Z 550 was equipped with two 150 mm cathodes of nickel and carbon. The cathodes were in side-by-side configuration as shown in Fig. 9. Multilayer structure was deposited in radio frequency mode (13.56 MHz), and the distances of the 48mm between the targets and the rotating substrate holder were held constant. The deposition rates were evaluated from the film thickness using Talystep profilometer. Argon was introduced into chamber and regulated by HI-TEC mass - flow controller (F-100) with the reproducibility of 0.2%. The total sputtering pressure measured with MKS A270B was approximately 0.2 Pa. The computer software was developed to keep argon pressure constant and to vary the flow of argon. For the deposition of the multilayer x-ray mirrors with resonant absorption the lateral fractional variation of the thickness inside the working area must be very small (less than 0.2%) and thus the whole deposition system (i.e. gas pressure, radio-frequency power, rotation speed etc..), must be stable within a tenth of a percent. Practical experiments on our equipment show that such stability is, at least during the time of the deposition, obtainable.

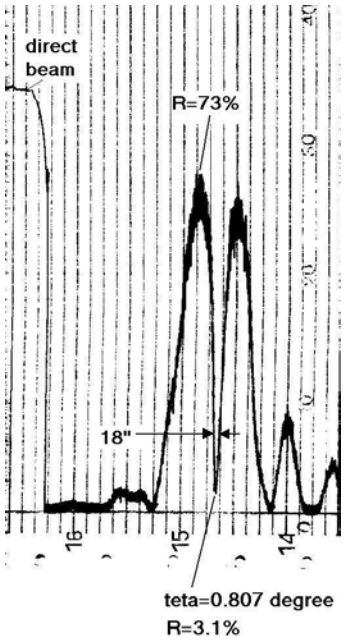

Fig.10. Reflection curve of the mirror. The angular axis is directed from right to left.

Reflection curve of the mirror measured in the angular region around the resonance is presented in Fig.10. It is very similar to the theoretical curve shown in Fig.5 that proves that the deposition process was close to optimal. Thus, manufacturing of the multilayer mirrors with a sufficiently deep and narrow resonant dip in the angular reflection curve is practically feasible.

5.2. Parallel and monochromatic probe x-ray beam

Estimations made in our previous paper [3] show that the divergence of the probe beam must not exceed 10 arc seconds. Apart of the divergence, the spectral width of the probe beam also plays a significant role because the mirror's resonant angle depends on the wavelength. The natural relative spectral width of the CuK_α doublet including side wings is of the order of $4 \cdot 10^{-3}$. Calculations show that such spectral widening increases the angular width of the resonance by a value of approximately 10 arc seconds. Therefore, the probe beam must have not only extremely small divergence, but good spectral purity as well. We have created the necessary probe beam using a standard 1.5 kW x-ray tube with a copper anode and long, fine focus coupled with a double crystal monochromator working in a strongly dispersive mode with both Si (111) reflections. The tube was installed in a point projection mode so as to form a point-like x-ray source with visible dimensions 0.8×0.4 mm^2. In this configuration, the horizontal divergence of the probe beam is equal to 7.4 arc seconds [7], while the relative spectral width is approximately $5 \cdot 10^{-4}$, i.e., an order of magnitude less than the natural spectral width of the CuK_α radiation. Thus, the effect of spectral widening can be neglected. The vertical divergence of the probe beam was of the order of several degrees.

5.3. Position Sensitive Detector

One of the key elements of the proposed refraction-contrast method is a high spatial resolution photon counting detector. Our recent work led to substantial improvements in the readout systems of position sensitive photon counting detectors with Microchannel Plates (MCPs) [8,9]. The spatial resolution of readout systems was improved from typical values of about ~20 μm FWHM to about 3-4 μm FWHM. Moreover, the progress in the detector readout has led not only to better spatial resolution, but also to substantial increase in detector counting rate capabilities. We are currently designing a system, which will be able to register more than 10^6 photons per second.

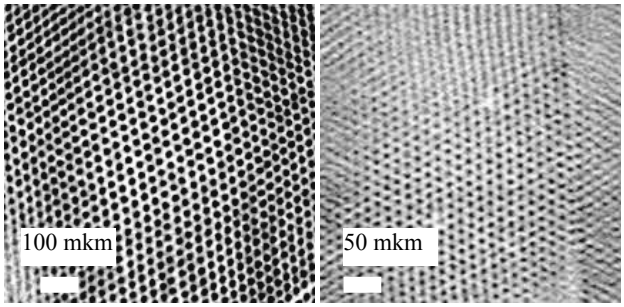

Fig. 11. Image of a small section of the cross strip MCP detector obtained with uniform illumination, showing the MCP pores and hexagonal multi-fibers. The bar across the images is 100 μm and 50 μm Left: MCP gain 5.5 x 10^6, MCP pair with 12.5μm pores, and 80:1 pore length/diameter ratio. Right: MCP gain 1.5 x 10^6, MCP pair with 7μm pores, and 80:1 pore length/diameter ratio.

Detectors with microchannel plates have been widely used for many applications, ranging from space based astrophysical imaging to synchrotron radiation research to biological autoradiography and many others. In these detectors a photon impinging on a photocathode deposited on the microchannel plate or on the input window is converted with some quantum efficiency into an electron. Various materials can be used as photocathodes to provide optimal sensitivity to different wavelength ranges. The photoelectron is then multiplied within a microchannel pore (thus preserving the position of the registered photon within the pore diameter) and the resulting charge cloud is collected by the readout anode, which encodes the position of the event. Typically MCP's in stacks of 2 or 3 provide amplification of 10^5 to > 10^7 gain while maintaining spatial information, determined by the channel diameter (currently in the range of 2 μm to 12 μm). Accuracy of the position encoding system previously was limiting the detector resolution to about 20 μm FWHM.

A novel detector readout scheme developed at the Space Sciences Laboratory, University of California at Berkeley - the cross strip (XS) anode [8,9] – led to substantial improvements in the overall detector performance, in particular detector spatial resolution and counting rate capabilities. The cross strip anode has a coarse (0.5mm) multilayer metal and ceramic cross strip pattern that encodes event positions by direct sensing of the charge from microchannel plate on each strip and subsequent determination of the charge cloud centroid for each event. Event position encoding is accomplished with chip level preamplifiers on the anode, subsequent analog to digital conversion of individual strip charge values and a software centroid determination. The anode responds in an event driven mode, each event results in an encoded X-Y position, time tag and signal amplitude. There is no "frame" readout encumbrance.

To date the XS scheme has been tested with an 8x8 mm^2 prototype (which we are currently extending to 25mm and 40mm formats) and laboratory electronics. We used MCPs with 7 and 12 μm pore diameters in these measurements and plan to replace them with microchannel pates with smaller pore diameters, which are available now [10] .

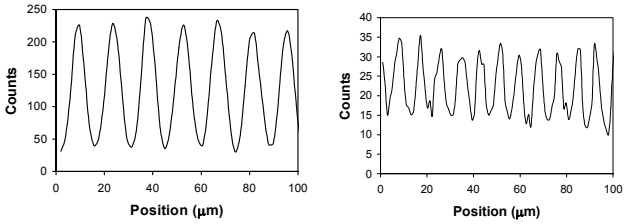

Fig.12. Histograms for a slice through pore images shown in Fig. 11 (left for 12.5 μm pores and right for 7 μm pores) showing about 3 μm FWHM spatial resolution.

The results of our measurements with XS anode are shown in Fig.11 and Fig. 12. The images shown in these figures are obtained with full field uniform illumination. The spatial resolution of the detector in that case was limited by the MCP pore size. However, these tests allow us to study the spatial sensitivity of the readout system in the entire detector active area, since in that case microchannel plate is not only providing the photoelectron multiplication, but also serves as a test mask. Figs. 11 and 12 show that each pore in microchannel plate is imaged by the anode individually. Cross sections through the images, shown in Fig. 12 clearly verify that the XS anode performance (~3μm FWHM) exceeds the spatial resolution of existing direct charge sensing anodes with equivalent sized formats, and does so at lower gain (<1.5 x 10^6). The image linearity was found to be very good so that it enabled distortions in the microchannel plate hexagonal boundaries to be seen.

The fact that cross strip anode can achieve this high spatial resolution with low MCP gain (˜1.5 x 10^6) provides opportunity to increase the local counting rate and overall detector lifetime. Our further goals are to combine the XS anode with 2-3μm pore MCP's for high resolution imaging tests, which should provide the total detector spatial sensitivity of just few microns. At the same time we are developing new low power amplifier chips with the preamplifier, shaper, discriminators and signal latching. These, combined with high speed CMOS ADC's and a centroid

algorithm performed by high speed Digital Signal Processor chips should enable detector operation with counting rates as high as > 1MHz.

6. INITIAL EXPERIMENTAL RESULTS

The scheme of the experiment is presented in Fig.13. The refracted (and, therefore, deflected from their original direction) components of the probe beam passed through the object placed immediately after the monochromator were efficiently reflected by a multilayer mirror positioned at a resonant grazing angle of 0.8° with respect to the probe beam, while the direct component was strongly attenuated. The output intensity distribution was measured in the mirror's plane of incidence by a linear detector array composed of 2580 reverse biased silicon photodiodes with individual amplifiers. Each sensitive element has the dimensions of

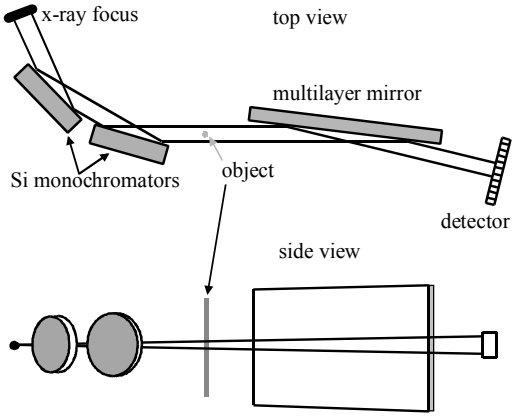

Fig.13. Optical scheme of the experiment.

1×0.01 mm^2, and the spacing between the elements is equal to 2.5 μm. Thus, the geometrical spatial resolution of the detector is 12.5 μm, while its real resolution, taking into account the cross-talk between the neighboring sensitive elements, is about 20 μm. The sensitive array is assembled on a silicon substrate which is cooled and stabilized to a temperature of approximately 5C° with a Peltier refrigerator. The dark current and gain differences between single photodiodes are compensated for by taking into account the reference values measured and stored beforehand in the computer memory.

The signal-to-noise ratio was the crucial issue in the experiment. The inner noise of the detector has two components: variations of the average current drain from different sensitive elements and shot noise. The first component can be compensated for by subtracting the average output noise signal stored in the computer before measurements from the real-time signal. The second one can be reduced by averaging the output signal over both time and the number of realizations. The averaging time interval was limited by the charge leakage current, and in the experiment could not exceed 1 second. Additional averaging over 100 realizations was applied, so that the total duration of one measuring cycle was 100 seconds.

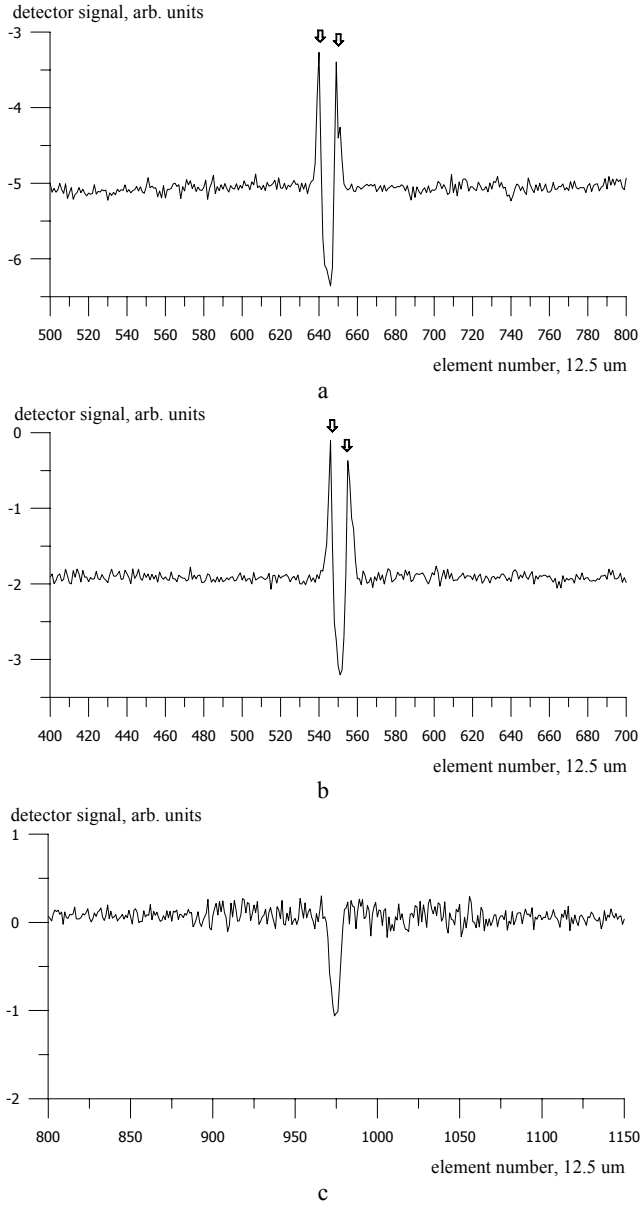

Fig.14. One-dimensional images of a copper wire 75 μm in diameter: (a),(b) refraction-contrast mode; (c) absorption mode. The refraction-contrast peaks are marked with arrows.

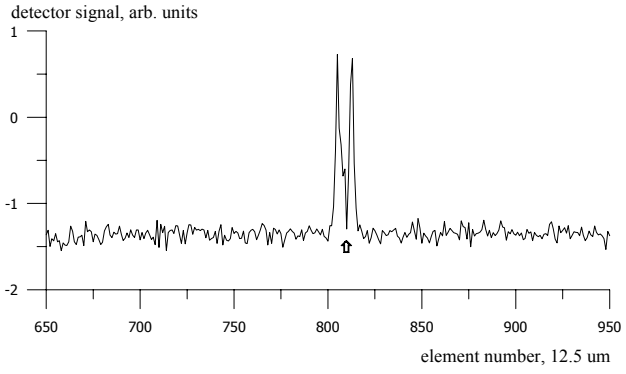

a

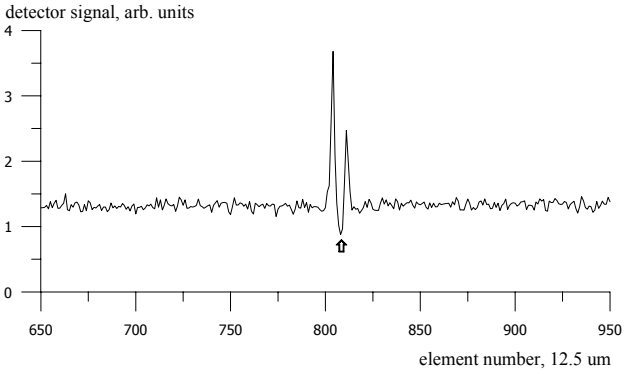

b

Fig.15. One-dimensional refraction-contrast images of different human hairs. Absorption dips are marked with arrows.

Two types of objects were used in the experiment: a copper wire 75 μm in diameter and a human hair approximately 60 μm in diameter. The experimental results obtained with a copper wire are presented in Fig.14a,b in two arbitrarily chosen realizations. The central dip emerges due to absorption, while two side peaks of the opposite sign marked by the arrows arise due to refraction. In order to prove that the marked regions really correspond to a refraction contrast the multilayer mirror was removed from the probe beam, thus leaving the optical path to the detector free (Fig.14c). One can distinctly see the absence of side reflexes in this case. This mode of operation corresponds to traditional absorption radiography.

A human hair is a far less absorbing object with respect to a copper wire at CuK_α radiation. Therefore, as can be seen from Fig.15a, the central dip, originating from absorption contrast, cannot be recognized on the background of the detector shot noise. Thus, the detector couldn't identify the presence of this hair on the background of its noise if it worked in the absorption-contrast mode. However, in the dark-field refraction-contrast mode the two side peaks are clearly seen. A different type of human hair is shown in Fig.15b. Here the absorption dip is larger than in the previous case, though it is still far less than the refraction contrast peaks. Supposedly this situation corresponds to a stronger absorption of X rays in the material of the hair due to the presence of heavy elements. Thus, even such simple experimental arrangement as described above can give interesting analytical information.

7. CONCLUSIONS

Many groups throughout the world are attempting to create an operating facility for x-ray refraction radiography using both synchrotron and laboratory-based sources. A new approach to development of a laboratory-based facility using multilayer mirrors with resonant absorption was introduced in our previous publication [3]. Now, we have experimentally proved that this method is capable of observing as small objects as human hairs. We have experimentally demonstrated the possibility of creating the critical components for this method: a multilayer mirror with resonant absorption, a probe beam with the necessary divergence, and an x-ray detector with necessary spatial resolution, working in the photon-counting mode. In the nearest future we are planning to create the working prototype of the laboratory device on the principle of the dark-field refraction contrast imaging.

ACKNOWLEDGEMENTS

The authors are grateful to Dr. A.A. Lomov and to Prof. R.M. Imamov from the Institute of Crystallography, Russian Academy of Sciences, for their generous help and support of this work, and to Z.Bochnicek from Masaryk University, Brno, Czech Republic, for his assistance in x-ray measurements.

REFERENCES

1. V.N.Ingal, and E.A.Beliaevskaya, "Imaging of biological objects in the plane-wave diffraction scheme", *Il Nuovo Cimento* **19D**, pp.553-560, 1997.
2. V.A.Bushuev, E.A.Beliaevskaya and V.N.Ingal, "Wave-optical description of x-ray phase contrast images of weakly absorbing non-crystalline objects", Il *Nuovo Cimento* **19D**, pp.513-520, 1997.
3. V.V. Protopopov, "On the possibility of x-ray refractive radiography using multilayer mirrors with resonant absorption", *Opt. Commun.* **174**, pp.13-18, 2000.
4. V.V.Protopopov, V.A.Kalnov, "Observation of x-ray refraction contrast using multilayer mirrors with resonant absorption", *Opt. Commun.* **184**, pp.1-6, 2000.
5. S.DiFonzo, W.Jark, G.Soullie, A.Gedola, S.Lagomarsin, P.Cloetans, C.Rickel, Journ. Synchrotron Radiat. 5, Pt.3 (1998) 376.
6. V.V.Protopopov, V.A.Kalnov, "X-ray multilayer mirrors with an extended angular range", *Opt. Commun.* **158**, pp.127-140, 1998.
7. R.Caciuffo, S.Melone, F.Rustichelli, and A.Boeuf, "Monochromators for x-ray synchrotron radiation", *Phys. Rep.* **152**, pp.1-70, 1987.
8. O.H.W. Siegmund, A.S. Tremsin, J.V. Vallerga and J. Hull, "Cross strip imaging anodes for microchannel plate detectors", *IEEE Trans. Nucl. Sci.* **48** pp.430-434, 2001.
9. O.H. W. Siegmund, A. S. Tremsin, R. Abiad, J. V. Vallerga, "Cross-strip anodes for microchannel pate detectors", *Proc. SPIE* vol. **4498**, “UV/EUV and Visible Space Instrumentation for Astronomy and Solar Physics”, pp.131-140, 2001.
10. B. Laprade, R. Starcher, “Development of a 2-mu m-pore microchannel plate”, *Spectroscopy* **16** (10) p.34 2001.